The 2nd Iranian Conference on Microelectronics (ICM2020)
23 – 25 December 2020

An Efficient Dual-Resonance Inductive Link for Biomedical Implants

Farshad Gozalpour
Integrated Circuits Design Laboratory, Department of Electrical Engineering, Amirkabir University of Technology (Tehran Polytechnic), Tehran, Iran.
Email: f.gozalpour@aut.ac.ir

Mohammad Yavari
Integrated Circuits Design Laboratory, Department of Electrical Engineering, Amirkabir University of Technology (Tehran Polytechnic), Tehran, Iran.
Email: myavari@aut.ac.ir

***Abstract*— In this paper, a dual-band inductive link has been designed which has high efficiency at two different frequencies and is suitable for FSK modulation in biomedical applications. The electrical parameters of the coils have been extracted using their 2-dimensional (2-D) axisymmetric modeling in COMSOL Multiphysics. With this model, the number of meshes required in finite element method is reduced, which decreases the simulation time. Using circular PCB coils as the main coils with outer diameter of 25.5 mm, and compact solenoids as lumped inductance with only 3.22 mm of winding diameter, simulated power transmission efficiency (PTE) at 6.78 MHz and 13.56 MHz, is 69.8% and 89.26%, respectively. Also, the power delivered to load (PDL) for R_L = 50 Ω is 51.6 mW and 53.58 mW at 6.78 MHz and 13.56 MHz, respectively. The coupling coefficient (k) of 0.308 that is obtained for the coil separation of 6 mm in Ansys Maxwell, has been used in simulations.**

Keywords*— *dual-resonance inductive link, wireless power transfer (WPT), power transmission efficiency (PTE), power delivered to load (PDL), biomedical implant

I. Introduction

Implantable medical devices (IMD), with the main purpose of improving the body's organs with unusual performance, have attracted special attention in recent years. They include pacemaker [1], brain-machine interface (BMI) [2, 3], retinal prosthesis [4], cochlear implant [5], etc. The first biomedical product implanted in the body was the Greatbatch's pacemaker and developed in 1958. The use of batteries to provide the power in IMDs requires periodic surgery due to limited battery life-time. Meanwhile, wireless power transfer (WPT) provides a continuous and safe operation of IMDs without the need for wires passing through the skin that cause infection. As a result, the wireless operation of IMDs is essential to prevent infection and human comfortability.

There are several strategies to implement WPT systems: near-field capacitive coupling (NCC) [6], ultrasonic [7], and near-field resonant inductive coupling (NRIC) [8]. In NCC, the impedance caused by the capacitive reactance between transmitter and receiver is high, even for a small distance between the plates, and the current drawn from the source is negligible. As a result, NCC has lower power transmission capacity. In ultrasonic, sound waves with frequencies higher than 20 kHz are used to transmit energy in physical environment (not vacuum). The acoustic impedance is very high for bone and therefore, this method is used only in certain areas of the body without bones.

NRIC is the oldest and predominant method of wireless transmission that can provide the power required by most biomedical systems (from a few milliwatts to several tens of milliwatts) with high reliability, safety, and efficiency. This method is based on electromagnetic waves. The primary coil (transmitter) that is placed on the skin, generates a time-varying magnetic field, and the electromagnetic force is induced in the secondary coil (receiver) which is located inside the body. Since the distance between coils is comparable to the dimensions of them, there is a poor coupling between coils, and only a fraction of the magnetic field is received in the receiver side.

Power transmission efficiency (PTE) is one of the most important parameters in evaluating the performance of wireless systems. PTE optimization in WPT systems is essential to reduce the size of the external energy source, the heat loss of coils inside the body tissue, and lowering the interference with other systems. By increasing efficiency, the external battery life-time is increased and the maximum allowable amount of AC magnetic field passing through the tissue, which is determined by international standards, is observed. In practice, coil losses (due to skin effect), poor coupling (due to the misalignment and significant separation of the coils), impedance mismatching in transmitter and receiver sides, tissue loss, etc., reduce PTE. The first essential step in increasing the PTE is to use LC resonance structures in transmitter and receiver sides with a resonance frequency equal to the driver frequency. At this frequency, the impedance of the LC tanks is pure resistive without any reactive power.

In WPT systems, simultaneous achievement of high efficiency continuous power transmission along with high-rate bidirectional data path is a challenging process. This challenge becomes even more difficult in modulations such as FSK that require two carriers. In order to reduce this challenge, the power and data transmission paths can be separated and each of them can be designed to meet the desired needs. In these architectures, the amplitude of the power carrier is more than twice the data carrier amplitude and as a strong interference, reduces the signal-to-noise ratio in the data receiver coil and increases the bit error rate. In other words, the data signal is saturated before it is received by the receiver [9]. Various implementations have been proposed to reduce these interferences, such as coplanar [9], coaxial [9], orthogonal [10], and figure-8 [10]. However, due to misalignments and limited space, the interference and cross-talk will not be completely removed. Also, due to the limited space in the body, the large occupied space of the

implant coils is another major disadvantage of multi-link systems.

The disadvantages mentioned above encourage us to transfer power and data using only one inductive link. In [11], using switches, the capacitor of the load network as well as the capacitor parallel to the switch of power amplifier are switched according to input data '0' and '1'. This is done to create two different resonance frequencies for FSK modulation. This mechanism has been used just in transmitter side and cannot be used for the secondary side because the receiver is not aware of the input data before it is received. Thus, unlike the primary side, the secondary side of the link has only one resonance frequency and the obtained efficiency without considering the rectifier and regulator is equal to 25%. In [12] using the combination of series and parallel LC tanks in the primary side of the link, two resonance frequencies are obtained, but the secondary side has only one resonance frequency, and the efficiency has been reduced to 20%.

II. Dual-Resonance Inductive Link

Fig. 1(a) shows the equivalent circuit of a dual-resonance coil, which is a combination of an LC branch and an LC tank, and results in two resonance frequencies. The compact capacitor C_1 is connected to the main coil L_1 to obtain the LC branch. The LC tank is also obtained by parallel combination of C_2 and compact inductance L_2. The LC tank behaves inductively when the operating frequency is lower than its resonance frequency (Z_2 is inductive), and behaves capacitively when operating frequency is higher than its resonance frequency [13]. Low resonance frequency is obtained by combining the LC branch and inductive LC tank, and high resonance frequency is obtained by combining the LC branch and capacitive LC tank. The resonance frequencies of dual-resonance coil are as follows [13]:

$$\begin{cases} f_{o1} = f_{oLC1}\sqrt{\frac{1}{2}+\frac{r_C}{2}\left(1+r_L-\sqrt{\left(\frac{r_L r_C-1}{r_C}\right)^2+2\left(\frac{r_L r_C+1}{r_C}\right)+1}\right)} \\ f_{o2} = f_{oLC1}\sqrt{\frac{1}{2}+\frac{r_C}{2}\left(1+r_L+\sqrt{\left(\frac{r_L r_C-1}{r_C}\right)^2+2\left(\frac{r_L r_C+1}{r_C}\right)+1}\right)} \end{cases} \quad (1)$$

Where f_{oLC1} is resonance frequency of LC branch, r_L is inductance ratio of L_1/L_2, and r_C is capacitive ratio of C_1/C_2 (Fig. 1(a)). f_{oLC1} and f_{oLC2} must be between f_{o1} and f_{o2}. f_{oLC2} is resonance frequency of the LC tank. The resulting bandwidth allows both carriers of the FSK modulation to pass through the link and sufficient energy will be transferred to the load.

Fig. 1(b) illustrates the schematic of dual-resonance WPT link made of dual-resonance coils. In this link, L_1 and L_2 are the main coils with coupling coefficient of k_{12}. L_3 and L_4 are the mentioned compact inductances and have no coupling with any element. Therefore, all of the coefficients k_{31}, k_{32}, k_{34}, k_{41}, and k_{42} are zero. Also, due to the use of a single inductive link, no unwanted interference and cross-talk will happen. The idea of dual-resonance coils is suggested in [13], but the link is not designed for biomedical applications, and the single turn coils with diameter of 20 cm are used as the main coils.

In ISM band, 13.56 MHz is one of the most widely used frequencies due to establish of a balance between coil size, switching loss, and tissue loss. In this paper, using dual-resonance coils, a dual-resonance inductive link is designed

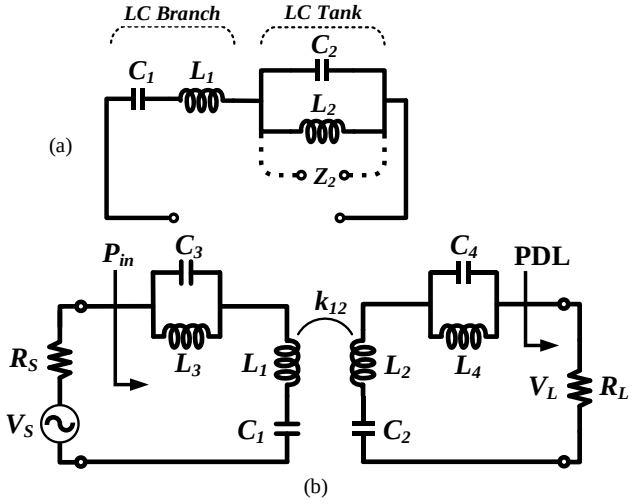

Fig. 1 (a) Dual-resonance coil, (b) Dual-resonance inductive link.

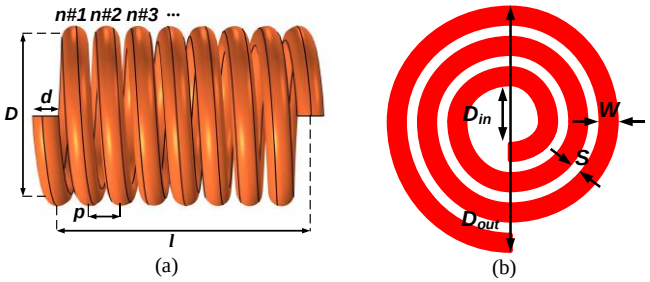

Fig. 2 Geometric parameters of solenoids and PCB circular coils (a) L_3, L_4, (b) L_1, L_2.

TABLE I. Geometric Parameters of The Coils

Parameters	PCB Coils L_1, L_2	Parameters	Solenoids L_3, L_4
D_{out} (mm)	25.5	D (mm)	3.22
D_{in} (mm)	11.1	d (mm)	0.2
W (mm)	0.3	p (mm)	0.22
S (mm)	0.3	l (mm)	9.46
n	12	n	43

for biomedical applications at 6.78 MHz and 13.56 MHz. According to these considered carriers and also 9.588 MHz for f_{oLC1} and f_{oLC2}, (1) gives the values of 2 and 0.5 for r_L and r_C, respectively. PCB circular coils and compact solenoids are used as the main coils and compact inductances, respectively.

III. Electrical Parameters

In this section, the electrical parameters of the coils are calculated. Fig. 2 shows the geometric structure of circular PCB spiral coils $L_{1,2}$, and solenoids $L_{3,4}$. PCB coils are very useful for implantation under the skin or epidural area due to their high flexibility in optimizing geometry and dimensions. The geometric design parameters of these coils are listed in Table I. Parameters D_{out}, D_{in}, W, S, and n illustrate outer diameter, inner diameter, trace width, trace spacing, and number of turns, respectively. Similar to FR-4 PCB, thickness of the conductor layer is considered to be 35 µm. Also, D, d, p, l, and n are parameters of the solenoids and represent winding diameter (distance from center to center of the wire), wire diameter, winding pitch, winding length, and number of turns, respectively. p is slightly bigger than d due to the insulation layer of the wire. (D , l) = (3.22 mm, 9.46 mm) for solenoids, make them suitable for implantation in body.

The electrical model of the coils include inductance, AC

resistance and a parallel capacitance. These elements are affected by the geometry, composition of the materials, as well as the surrounding environment of the coils.

For the PCB circular coils, the inductance can be determined by [14, 15]:

$$L = \frac{\mu_0 n^2 d_{avg}}{2}\left(\ln\left(\frac{2.46}{\beta}\right) + 0.2\beta^2\right) \quad (2)$$

Where μ_0 is the permeability of the free space, $d_{avg}=0.5(D_{out}+D_{in})$ is the average diameter of the coil, and $\beta=(D_{out}-D_{in})/(D_{out}+D_{in})$ is the fill-factor. Using (2), L of 3.1 µH is obtained for L_1 and L_2.

In [16], an expression is given for solenoids:

$$L = \frac{\mu_0 \pi r^2 n^2 \kappa}{l} \quad (3)$$

Where κ is the Nagaoka's coefficient and $r = D_{eff}/2$. D_{eff} is the effective diameter of the solenoid. The result for L_3 and L_4 with the reported parameters in table I is 1.6 µH.

Skin effect is the main source of AC resistance in conductors which is caused by high frequency current flow through them. For the case of PCB spirals, the skin effect loss R_{skin} is given by [15, 17]:

$$R_{skin} = R_{DC}\frac{t_0}{\delta\left(1-e^{-\frac{t_0}{\delta}}\right)}\frac{1}{1+\frac{t_0}{W}} \quad (4)$$

Where t_0 is trace thickness, $\delta = \sqrt{2\rho/\omega\mu_0}$ is skin depth, and $R_{DC}=\rho l_C/A$ is DC resistance. l_C is the conductor length. The result for PCB coils at 6.78 MHz and 13.56 MHz is 1.86 Ω and 2.3 Ω, respectively.

For the case of solenoids L_3 and L_4, the AC resistance is given by [18]:

$$R_{ac} = \frac{\rho l_w}{\pi\left(d\delta-\delta^2\right)}\Phi\frac{n-1}{n} \quad (5)$$

Where Φ is the proximity factor interpolated from empirical Medhurst data, and l_W is the effective wire length. Using (5) R_{ac} at 6.78 MHz and 13.56 MHz is 1.7 Ω and 2.3 Ω, respectively.

In [19] an approximation for parasitic capacitance of PCB coils is given:

$$C_p \approx \left(\alpha\varepsilon_{rc}+\beta\varepsilon_{rs}\right)\varepsilon_0\frac{t_0}{S}l_g \quad (6)$$

Where ε_{rc} and ε_{rs} are the relative dielectric constants of coating and substrate, respectively. l_g is the length of gap between traces and can be calculated for circular coils. For the case of air and FR-4 PCB, $(\alpha\ ,\beta) = (0.9\ ,\ 0.1)$ and $(\varepsilon_{rc}\ ,\ \varepsilon_{rs}) = (1\ ,\ 4.4)$ [19]. Using (6), C_p of 0.889 pF is obtained for L_1 and L_2.

Medhurst formula gives a simple expression for self-capacitance of the solenoids in pF/cm [20, 21]:

$$\frac{C}{D} = 0.1126\frac{l}{D} + 0.08 + 0.27\sqrt{\frac{D}{l}} \quad (7)$$

The calculated value will be 0.57 pF/cm for L_3 and L_4. Of course, Medhurst formula overestimates the parasitic capacitance for solenoids with no former and small l/D.

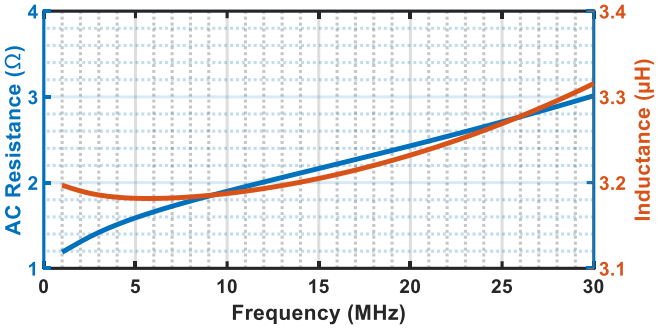

Fig. 3 Simulated inductance and AC resistance of PCB coils.

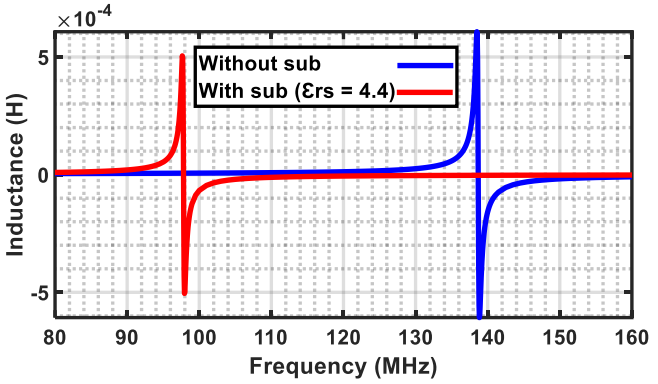

Fig. 4 Simulated self-resonance frequency of PCB coils for ε_{rs} of 1 and 4.4.

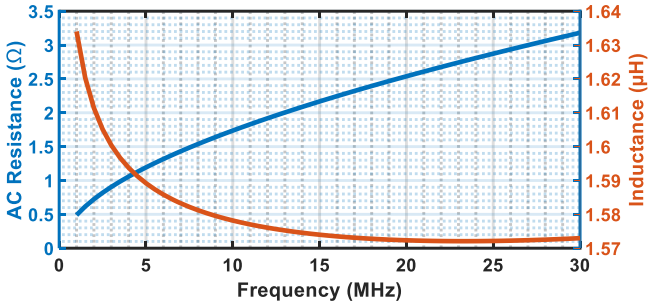

Fig. 5 Simulated inductance and AC resistance of solenoids.

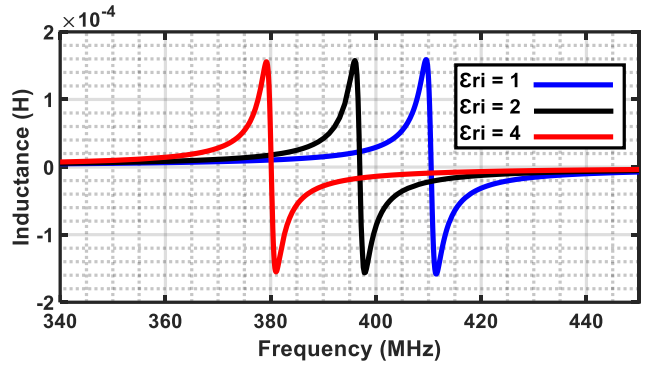

Fig. 6 Simulated self-resonance frequency of solenoids for ε_{ri} of 1, 2, and 4.

IV. Simulation Results

In order to perform electromagnetic simulations of the coils by finite element method, COMSOL software has been used and a 2-D axisymmetric model has been drawn for them to extract the electrical model. The use of this model reduces the number of meshes and as a result, the simulation time is reduced.

Fig. 3 shows the simulated inductance and AC resistance of PCB coils L_1 and L_2 in the range of 1 MHz to 30 MHz. It is clear that there is a good agreement between the simulated

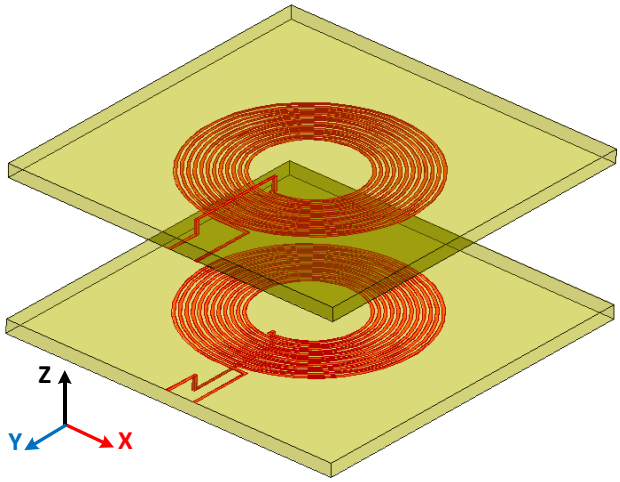

Fig. 7 Maxwell simulation setup of circular coils for coupling coefficient.

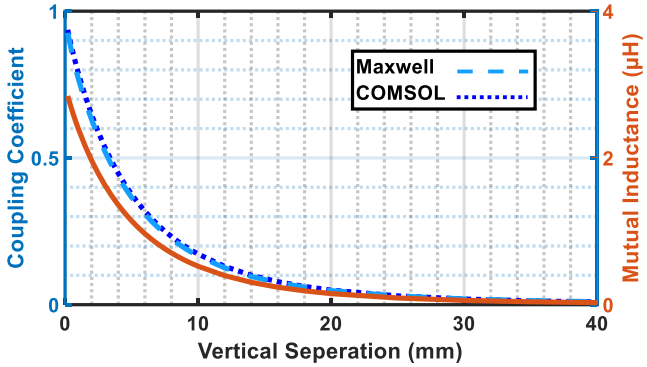

Fig. 8 Simulated coupling coefficient and mutual inductance between PCB coils for different vertical separations.

and calculated values, and as a result, the used 2-D model has extracted the electrical parameters of the coils with good accuracy. The self-resonance frequency (f_{SRF}) of L_1 and L_2 is also simulated for ε_{rs} of 1 and 4.4 and the result is shown in Fig. 4. The inductive behavior of the coils before f_{SRF} and capacitive behavior after f_{SRF} are known from the figure. The zero-crossing point specifies the f_{SRF}. As the ε_{rs} increases, this point moves to lower frequencies, indicating a direct ratio of ε_{rs} with parasitic capacitance. For ε_{rs} of 4.4, this point is equal to 97.8 MHz. Similar simulations have been performed for solenoids and the results are shown in Fig. 5 and 6, which are in good agreement with the calculations. For ε_{ri} of 2, f_{SRF} is equal to 396.9 MHz. ε_{ri} is the relative dielectric constant of insulator layer.

In order to simulate the coupling coefficient (k) between circular coils, their 3-D model is drawn in Maxwell environment (Fig. 7). The substrate thickness is assumed to be 1.5 mm. Fig. 8 shows the simulation results of the k and the mutual inductance (M) for vertical separation of 0.2 mm to 40 mm. As is clear, there is a very good matching between the results of 3-D Maxwell model and 2-D axisymmetric COMSOL model.

In order to simulate the electrical performance of the inductive link, an AC source with a series resistance (R_S) of 50 Ω is considered as the function generator, and load resistance (R_L) is assumed to be 50 Ω (Fig. 1(b)). According to the frequency response shown in Fig. 9, the value of V_L/V_S for k of 0.308 (separation of 6 mm between L_1 and L_2) at 6.78 MHz and 13.56 MHz is -7.66 dB and -7.49 dB, respectively. As a result, the amplitude of the received signal at both frequencies are almost equal and there will be no

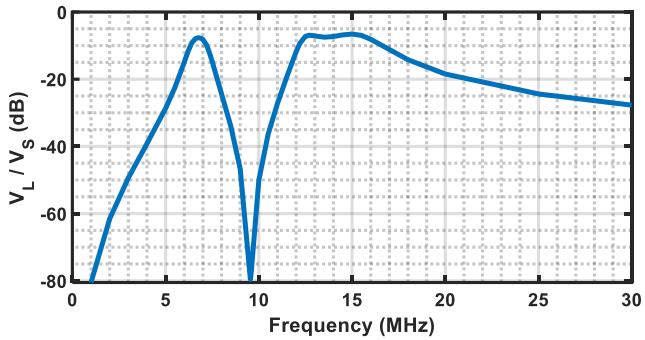

Fig. 9 Simulated V_L / V_S for the separation of 6 mm between coils.

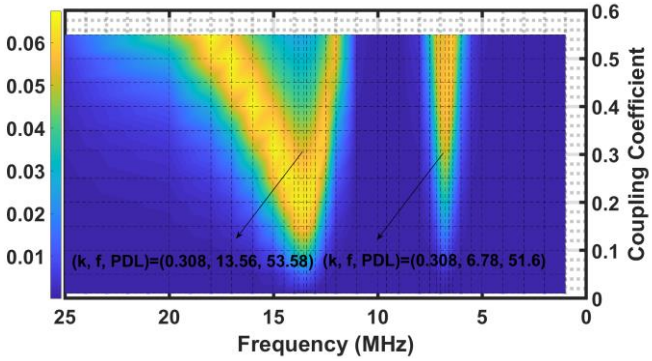

Fig. 10 Simulated PDL of the inductive link.

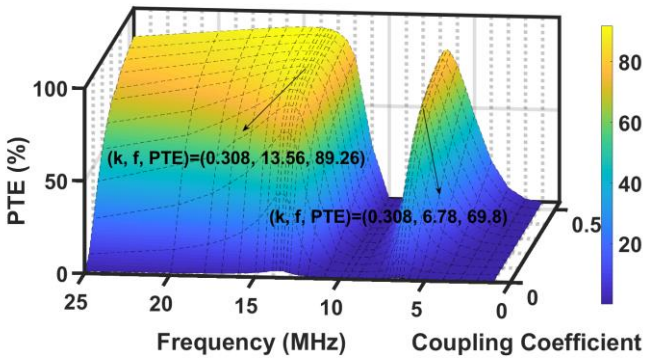

Fig. 11 Simulated PTE of the inductive link.

problem in detecting the modulated FSK signal in the receiver side.

Fig. 10 illustrates the PDL of the link as a function of k and frequency. The PDL at 6.78 MHz and 13.56 MHz for k = 0.308 and V_S = 11 V_{P-P} is 51.6 mW and 53.58 mW, respectively, which are sufficient for biomedical applications such as cochlear implants. PTE of the link, which is defined as the ratio of delivered power to the load, to the power drawn from the modelled function generator (PDL/P_{in}), is simulated in Fig. 11 as a function of k and frequency. The proportionality of PTE with k is well known from the figure. Also, at resonance frequencies of 6.78 MHz and 13.56 MHz, the stored reactive power in the system is minimized and therefore high efficiency is achieved.

V. Conclusion

In this paper, an efficient wideband inductive link that has two resonance frequencies at 6.78 MHz and 13.56 MHz has been designed. Circular shaped PCB coils with outer diameter of 25.5 mm and solenoids with winding diameter of 3.22 mm and winding length of 9.46 mm have been used as the main coils and lumped inductances, respectively. These dimensions make the link suitable for applications with limited implant space. Also, using 2-D axisymmetric

modeling in COMSOL environment, the electrical parameters of the coils have been extracted. High efficiency at both frequencies are obtained in simulation results. Assuming the same probability for data bits of '0' and '1', the average link efficiency for 6 mm of distance between coils, will be 79.53%. The power transmitted to the load at 6.78 MHz and 13.56 MHz is 51.6 mW and 53.58 mW, respectively, which makes the link suitable for applications with continuous power requirements.

REFERENCES

[1] C. Liu, C. Jiang, J. Song, and K. Chau, "An effective sandwiched wireless power transfer system for charging implantable cardiac pacemaker," *IEEE Transactions on Industrial Electronics*, vol. 66, no. 5, pp. 4108-4117, 2018.

[2] B. Lee, Y. Jia, S. A. Mirbozorgi, M. Connolly, X. Tong, Z. Zeng, B. Mahmoudi, and M. Ghovanloo, "An inductively-powered wireless neural recording and stimulation system for freely-behaving animals," *IEEE transactions on biomedical circuits and systems*, vol. 13, no. 2, pp. 413-424, 2019.

[3] J. P. Uehlin, W. A. Smith, V. R. Pamula, E. P. Pepin, S. Perlmutter, V. Sathe, and J. C. Rudell, "A Single-Chip Bidirectional Neural Interface With High-Voltage Stimulation and Adaptive Artifact Cancellation in Standard CMOS," *IEEE Journal of Solid-State Circuits*, 2020.

[4] P.-H. Kuo, O.-Y. Wong, C.-K. Tzeng, P.-W. Wu, C.-C. Chiao, P.-H. Chen, P.-C. Chen, Y.-C. Tsai, F.-L. Chu, and J. Ohta, "Improved charge pump design and ex vivo experimental validation of CMOS 256-pixel photovoltaic-powered subretinal prosthetic chip," *IEEE Transactions on Biomedical Engineering*, vol. 67, no. 5, pp. 1490-1504, 2019.

[5] N. Guo, S. Wang, R. Genov, L. Wang, and D. Ho, "Asynchronous Event-driven Encoder With Simultaneous Temporal Envelope and Phase Extraction for Cochlear Implants," *IEEE Transactions on Biomedical Circuits and Systems*, vol. 14, no. 3, pp. 620-630, 2020.

[6] R. Erfani, F. Marefat, S. Nag, and P. Mohseni, "A 1–10-MHz Frequency-Aware CMOS Active Rectifier With Dual-Loop Adaptive Delay Compensation and> 230-mW Output Power for Capacitively Powered Biomedical Implants," *IEEE Journal of Solid-State Circuits*, vol. 55, no. 3, pp. 756-766, 2019.

[7] M. M. Ghanbari, D. K. Piech, K. Shen, S. F. Alamouti, C. Yalcin, B. C. Johnson, J. M. Carmena, M. M. Maharbiz, and R. Muller, "A Sub-mm 3 Ultrasonic Free-Floating Implant for Multi-Mote Neural Recording," *IEEE Journal of Solid-State Circuits*, vol. 54, no. 11, pp. 3017-3030, 2019.

[8] X.-H. Qian, Y.-C. Wu, T.-Y. Yang, C.-H. Cheng, H.-C. Chu, W.-H. Cheng, T.-Y. Yen, T.-H. Lin, Y.-J. Lin, and Y.-C. Lee, "Design and In Vivo Verification of a CMOS Bone-Guided Cochlear Implant Microsystem," *IEEE Transactions on Biomedical Engineering*, vol. 66, no. 11, pp. 3156-3167, 2019.

[9] G. Wang, P. Wang, Y. Tang, and W. Liu, "Analysis of dual band power and data telemetry for biomedical implants," *IEEE Transactions on biomedical circuits and systems*, vol. 6, no. 3, pp. 208-215, 2011.

[10] U.-M. Jow, and M. Ghovanloo, "Optimization of data coils in a multiband wireless link for neuroprosthetic implantable devices," *IEEE transactions on biomedical circuits and systems*, vol. 4, no. 5, pp. 301-310, 2010.

[11] M. M. Ahmadi, and S. Ghandi, "A Class-E Power Amplifier With Wideband FSK Modulation for Inductive Power and Data Transmission to Medical Implants," *IEEE Sensors Journal*, vol. 18, no. 17, pp. 7242-7252, 2018.

[12] M. Ghovanloo, and K. Najafi, "A wideband frequency-shift keying wireless link for inductively powered biomedical implants," *IEEE Transactions on Circuits and Systems I: Regular Papers*, vol. 51, no. 12, pp. 2374-2383, 2004.

[13] M.-L. Kung, and K.-H. Lin, "Enhanced analysis and design method of dual-band coil module for near-field wireless power transfer systems," *IEEE Transactions on Microwave Theory and Techniques*, vol. 63, no. 3, pp. 821-832, 2015.

[14] S. S. Mohan, M. del Mar Hershenson, S. P. Boyd, and T. H. Lee, "Simple accurate expressions for planar spiral inductances," *IEEE Journal of solid-state circuits*, vol. 34, no. 10, pp. 1419-1424, 1999.

[15] M. Schormans, V. Valente, and A. Demosthenous, "Practical inductive link design for biomedical wireless power transfer: A tutorial," *IEEE transactions on biomedical circuits and systems*, vol. 12, no. 5, pp. 1112-1130, 2018.

[16] D. Knight, "An introduction to the art of solenoid inductance calculation," 2016.

[17] H. A. Wheeler, "Formulas for the skin effect," *Proceedings of the IRE*, vol. 30, no. 9, pp. 412-424, 1942.

[18] D. W. Knight, "Selonoid Impedance and Q" 2016. [Online]. Available: http://www.g3ynh.info/zdocs/magnetics/solenz.html.

[19] U.-M. Jow, and M. Ghovanloo, "Design and optimization of printed spiral coils for efficient transcutaneous inductive power transmission," *IEEE Transactions on biomedical circuits and systems*, vol. 1, no. 3, pp. 193-202, 2007.

[20] D. W. Knight, "The self-resonance and self-capacitance of solenoid coils. applicable theory, models and calculation methods," *G3YNH info*, vol. 10, 2016.

[21] R. Medhurst, "HF resistance and self-capacitance of single-layer solenoids," *Wireless Engineer*, vol. 24, 1947.